Biochimica et Biophysica Acta 1848 (2015) 932–941

Contents lists available at ScienceDirect

Biochimica et Biophysica Acta

journal homepage: www.elsevier.com/locate/bbamem

Channel-forming activity of syringomycin E in two mercury-supported biomimetic membranes

Lucia Becucci [a,*], Vania Tramonti [a], Alberto Fiore [b,d], Vincenzo Fogliano [b], Andrea Scaloni [c], Rolando Guidelli [e,1]

[a] Department of Chemistry, Florence University, via della Lastruccia 3, 50019 Sesto Fiorentino, Firenze, Italy
[b] Department of Agricultural and Food Science, University of Naples "Federico II", 80055 Portici, Italy
[c] Proteomics & Mass Spectrometry Laboratory, ISPAAM-National Research Council, 80147 Naples, Italy
[d] School of Science, Engineering & Technology, Division of Food & Life Sciences, Abertay University, Kydd Building, Dundee, DD1 1HG, UK
[e] Florence University, Italy

ARTICLE INFO

Article history:
Received 26 September 2014
Received in revised form 5 December 2014
Accepted 8 December 2014
Available online 29 December 2014

Keywords:
Lipodepsipeptides
Self-assembled monolayers
Tethered bilayer lipid membranes
Potential step chronocoulometry
Cyclic voltammetry

ABSTRACT

The lipodepsipeptide syringomycin E (SR-E) interacts with two mercury-supported biomimetic membranes, which consist of a self-assembled phospholipid monolayer (SAM) and of a tethered bilayer lipid membrane (tBLM) separated from the mercury surface by a hydrophilic tetraethyleneoxy (TEO) spacer that acts as an ionic reservoir. SR-E interacts more rapidly and effectively with a SAM of dioleoylphosphatidylserine (DOPS) than with one of dioleoylphosphatidylcholine (DOPC). The proximal lipid monolayer of the tBLM has no polar head region, being linked to the TEO spacer via an ether bond, while the distal monolayer consists of either a DOPC or a DOPS leaflet. The ion flow into or out of the spacer through the lipid bilayer moiety of the tBLM was monitored by potential step chronocoulometry and cyclic voltammetry. With the distal monolayer bathed by aqueous 0.1 M KCl and 0.8 μM SR-E, an ion flow in two stages was monitored with DOPC at pH 3 and 5.4 and with DOPS at pH 3, while a single stage was observed with DOPS at pH 5.4. This behavior was compared with that already described at conventional bilayer lipid membranes. The sigmoidal shape of the chronocoulometric charge transients points to an aggregation of SR-E monomers forming an ion channel via a mechanism of nucleation and growth. The ion flow is mainly determined by potassium ions, and is inhibited by calcium ions. The contribution to the transmembrane potential from the distal leaflet depends more on the nature of the lipid than that of the ion channel.

1. Introduction

Syringomycin E (SR-E) is a cyclic lipodepsipeptide produced by the bacterium *Pseudomonas syringae*, which exerts fungicidal/bactericidal activity both on plant- and human-associated pathogenic microbes [1,2]. A peculiar composition made also of uncommon D and L-amino acids (4-chlorothreonine, 2,4-diaminobutyric acid, 2,3-dehydro-2-aminobutyric acid and 3-hydroxyaspartic acid) determines its basic characteristics [3–5]. Molecular dynamics simulations based on NMR data in sodium dodecyl sulfate micelles point to a molecular structure with the peptide backbone resembling the seam of a tennis ball and bearing the 3-OH dodecanoic acid moiety in extended conformation. Two distinct regions can be easily recognized in SR-E structure, i.e. a small negatively charged portion and a larger positively charged area [5].

SR-E promotes the translocation of mono- and divalent ions across plasma membranes [6,7] and forms channels in bilayer lipid membranes [8,9]. A SR-E ion channel requires at least six peptide molecules for its formation [10,11] and shows a preferential selectivity for anions [10–13], which decreases with an increase in electrolyte concentration. This selectivity may be ascribed to the positive charge of the SR-E molecules at the mouth of the ion channel. Anion selectivity increases as the negative charge of the lipid bilayer decreases [10,14]. When the SR-E molecules are added at one side of a conventional bilayer lipid membrane interposed between two aqueous solutions (BLM), they are incorporated asymmetrically (with the lactone ring on the same side) and do not translocate to the opposite side for at least 6–7 h [13]. SR-E forms two types of channel having different sizes. The large channels have a conductance about 6-fold higher and a dwell time significantly greater than the small ones [13]. The identical ion selectivity of the two types of channel and the identical radius of their aqueous pores (~1 nm) strongly suggest that the large channels are just clusters of the small ones, with synchronized opening/closing [9,11,13]. These clusters seem stabilized electrostatically by negatively charged lipids, which are interposed between the positively charged small channel units. The probability of observing these clusters increases with an increase in the negative charge of the lipid and diminishes with increasing salt concentration [13]. The different effect

* Corresponding author. Tel.: +39 055 457 3095; fax: +39 055 457 3385.
E-mail address: lucia.becucci@unifi.it (L. Becucci).
[1] Former Professor.

http://dx.doi.org/10.1016/j.bbamem.2014.12.007
0005-2736/

of PEG200 after its addition at the *cis* or the *trans* side of a BLM incorporating the lipodepsipeptide suggests a conical shape of the SR-E channel, with the *cis* radius larger than the *trans* one [15,16].

The present work aims at investigating the behavior of SR-E in dioleoylphosphatidylcholine (DOPC) and dioleoylphosphatidylserine (DOPS) lipid environments bathed by aqueous 0.1 KCl at pH 3 and 5.4. To this end, two mercury-supported biomimetic membranes were employed, namely a lipid monolayer self-assembled on the mercury surface (SAM) and a tethered bilayer lipid membrane (tBLM). The latter biomimetic membrane consists of a monolayer of a thiolipid, called DPTL, with a phospholipid monolayer on top of it. The DPTL thiolipid consists of a tetraethyleneoxy hydrophilic chain terminated at one end with a lipoic acid residue for anchoring to the mercury surface, and covalently linked at the other end to two phytanyl chains mimicking the hydrocarbon tails of a lipid [17]. The hydrophobic interactions between the phytanyl chains and the overlying phospholipid monolayer give rise to a lipid bilayer interposed between the tetraethyleneoxy chain, called spacer, and the bulk aqueous solution. The spacer may accommodate a number of water molecules and ions, thus acting as an ionic reservoir. Mercury provides a defect free, fluid and readily renewable surface to the self-assembling tBLM. Moreover, it imparts to the lipid molecules of the whole bilayer a lateral mobility comparable with that of biomembranes. The free movement of lipid molecules enables mercury-supported tBLMs to react to the presence of proteins, charges and physical forces in a dynamic and responsive manner. A satisfactory fluidity allows these biomimetic membranes to reorganize upon interaction with external perturbations, mimicking the functionality of living cell membranes. In particular, lateral mobility enables Hg-supported tBLMs to incorporate bulky membrane proteins, such as the HERG potassium channel [18]. As distinct from Hg-supported tBLMs, gold-supported tBLMs do not meet the requirement of fluidity and lipid lateral mobility, because the thiolipid molecules are rigidly bound to the metal surface atoms [19,20]. Moreover, the hydration of the polyethyleneoxy moiety of thiolipids anchored to gold is low [21,22], while the incorporation of proteins with extramembrane domains requires a significant hydration of the spacer. Hg-supported tBLMs have been extensively employed in our laboratory for the investigation of ion channels [23–31].

2. Material and methods

SR-E was obtained from *P. syringae* culture broths and purified as already reported [5]. Peptide purity and quantity was checked by mass spectrometry, reverse-phase chromatography, and amino acid analyses, respectively [3,5]. Stock solutions of 8×10^{-4} M SR-E in DMSO were stored at 4 °C. Merck (Darmstadt, Germany); suprapur® KCl was baked at 500 °C before use to remove any organic impurities. Adenosine 5′-triphosphate disodium salt (ATP), dimethylsulfoxide (DMSO) and $CaCl_2$ from Sigma-Aldrich (St. Louis, MO, USA) and KH_2PO_4 and K_2HPO_4 from Merck were used without further purification. DOPC and DOPS were purchased in chloroform solution from Avanti Polar Lipids (Birmingham, AL, USA). The 2,3,di-O-phytanyl-sn-glycerol-1-tetraethylene-glycol-D,L-α lipoic acid ester thiolipid (DPTL) was provided by Prof. Adrian Schwan (Department of Chemistry, University of Guelph, Canada) [17]; stock solutions of this thiolipid were stored at −18 °C. Deionized water was distilled once and then redistilled from alkaline permanganate before its use.

All measurements were carried out with a home-made hanging mercury drop electrode (HMDE) described elsewhere [32]. A home-made glass capillary with a finely tapered tip (about 1 mm in outer diameter) was used. Capillary and mercury reservoir were thermostated at 25 ± 0.1 °C in a water-jacketed box to avoid any changes in drop area due to a change in temperature. The HMDE acted as the working electrode in a three-electrode system, with an Ag/AgCl (0.1 M KCl) reference electrode and a platinum coil counter electrode. Mercury-supported lipid SAMs were obtained by spreading a lipid solution in pentane on the surface of a buffered or unbuffered 0.1 M KCl aqueous solution, in an amount corresponding to about five phospholipid monolayers. After allowing the pentane to evaporate, the HMDE was immersed into the aqueous solution across the lipid film. This procedure gives rise to a lipid monolayer with the hydrocarbon tails directed toward the mercury surface and the polar heads directed toward the aqueous solution, thanks to the hydrophobic nature of the mercury surface. The lipid monolayer is at its equilibrium spreading pressure (45 mN m^{-1}), in equilibrium with the bulk phase of the surfactant, i.e., a floating crystal of the surfactant [33,34]. Mercury-supported tBLMs were obtained by tethering a monolayer of the thiolipid DPTL on the HMDE, upon keeping the mercury drop immersed in a 0.2 mg/mL DPTL solution in ethanol for about 20 min [26]. A phospholipid monolayer was then formed on top of the DPTL monolayer by a procedure analogous to that used for the preparation of mercury-supported lipid monolayers; it consisted in spreading a lipid solution in pentane on the surface of a 0.1 M KCl aqueous solution. Immersing the DPTL-coated mercury into the aqueous solution across the lipid film causes a lipid monolayer to self-assemble on top of the DPTL monolayer, thanks to the hydrophobic interactions between the alkyl chains of the phospholipid and those of the thiolipid. The tBLM was then subjected to repeated potential scans over a potential range from −0.20 to −1.20 V, while continuously monitoring the curve of the quadrature component of the current at 75 Hz against the applied potential, *E*, using AC voltammetry, until a stable curve was attained.

Impedance spectroscopy, potential-step chronocoulometry, AC and cyclic voltammetry measurements were carried out with an Autolab instrument PGSTAT12 (Echo Chemie, Utrecht, The Netherlands) supplied with FRA2 module for impedance measurements, SCAN-GEN scan generator and GPES 4.9007 software. Potentials were measured vs. a Ag/AgCl electrode immersed in the 0.1 M KCl working solution, and are referred to this reference electrode. Impedance spectra at DOPC SAMs were recorded from 10^{-2} to 10^{5} Hz over the potential range of stability of the SAM, i.e. from −0.3 V to −0.8 V. The absolute precision of the numerical values reported in what follows is of ±5 μC cm^{-2} for charge densities and of ±5 mV for applied potentials.

3. Results

3.1. Effect of SR-E on DOPC and DOPS SAMs

The intercalation of biomolecules within a Hg-supported lipid monolayer has a disorganizing effect, even if only that of separating the lipid molecules from each other. It is, therefore, interesting to compare this effect with that obtained by expanding a pure lipid-coated mercury drop. Fig. 1 shows the AC voltammogram of a DOPC SAM in an unbuffered 0.1 M KCl aqueous solution both before and after two consecutive expansions of the drop area. Over the potential region of minimum capacitance, which ranges from −0.20 to −0.80 V, the DOPC monolayer on the unexpanded mercury drop is impermeable to inorganic ions, whereas it becomes permeable outside this region. The *C* value over this region amounts to 1.8 μF cm^{-2}, namely twice the value for a solvent-free BLM [35]. At positive potentials, the region of minimum capacitance is delimited by a capacitance increase that precedes mercury oxidation. At negative potentials, it is delimited by a sharp pseudocapacitance peak that lies at about −1.02 V, followed by two further peaks at about −1.10 V and −1.35 V, as shown by the solid curve in Fig. 1. The first two peaks are ascribed to a cooperative reorientation of the lipid molecules, whereas the third one is due to their partial desorption [33]. The first peak results from surface defects that allow a practically uninhibited access of inorganic ions to the mercury surface, whereas the second peak results from nucleation and growth of the defects formed during the first peak, causing their coalescence. The drop expansion causes the first sharp peak to be replaced by a broad shoulder, whereas the second and third peaks are practically unaltered. The minimum capacitance varies proportionally to the drop

area A [35,36] without incorporation of water into the lipid monolayer, thus maintaining the dielectric constant ε of the film practically unaltered. The specific capacitance C of the film can be approximately expressed by the Helmholtz formula, $C = \varepsilon_0\varepsilon / d$, for a parallel plate capacitor, where d is the film thickness and ε_0 is the permittivity of free space. Noting that, for a constant volume $V = Ad$ of the lipid material, A is inversely proportional to d, the specific capacitance C of the expanded drop is directly proportional to its surface area A.

The first sharp peak of the unexpanded DOPC monolayer is due to an arrangement of the phosphorylcholine zwitterion coplanar to the monolayer, due to electrostatic interactions between trimethylammonium and phosphate groups of adjacent lipid molecules, with a resulting stabilization of the unprotonated form of the latter groups [37]. As the interfacial electric field forces the zwitterionic dipoles to align normally to the plane of the lipid SAM, it determines a "domino effect", whereby the trimethylammonium-phosphate dipoles formed by adjacent polar heads collapse like a falling row of dominoes. This cooperative effect occurs over the narrow potential range of the first pseudocapacitance peak. An expansion of the mercury drop weakens the electrostatic interactions between adjacent trimethylammonium and phosphate groups. Consequently, the alignment of the zwitterionic dipoles along the direction of the electric field occurs independent of each other, over the broader potential range covered by the shoulder in Fig. 1. Apparently, this phenomenon does not affect the nucleation and growth of monolayer defects responsible for the second peak.

The AC voltammetry curve of an unexpanded mercury-supported DOPS monolayer in unbuffered aqueous 0.1 KCl differs from that of a DOPC monolayer by a broader region of minimum capacitance, which extends up to −1.10 V, and by the presence of two pseudocapacitance peaks [38]. Since the potential region negative of the first pseudocapacitance peak, which lies at about −1.20 V, is not entirely reproducible, only the first peak is shown in the solid curve of Fig. 2. The DOPS monolayer was shown to be positively charged at pH 3, almost neutral around pH 6 and negatively charged with a further increase in pH [37]. This behavior was tentatively explained by a conformation with the carboxyl and the amino groups of adjacent DOPS molecules coplanar to the monolayer and characterized by electrostatic dipole–dipole interactions. The phosphate group, whose pK is about 8, is buried inside the polar head region and is almost completely protonated at pH 6. The expansion of the DOPS-coated mercury drop causes a notable increase and a moderate broadening of the pseudocapacitance peak with an increase in drop area, as shown in Fig. 2. The drop expansion at potentials along the flat capacitance minimum is unlikely to expose the phosphate group to the aqueous solution, with its resulting

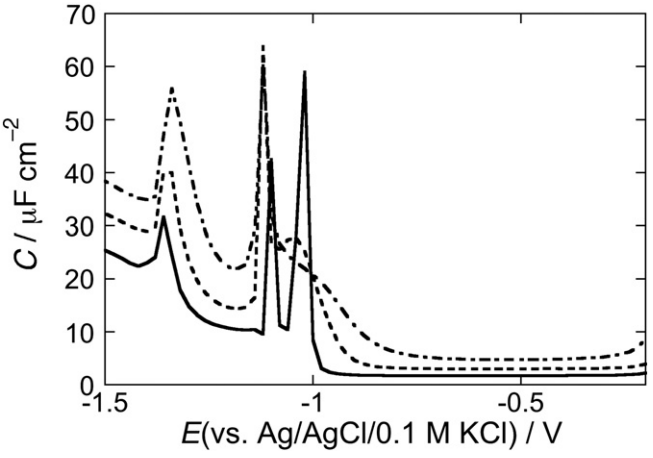

Fig. 1. AC voltammograms at 75 Hz of a Hg-supported DOPC SAM in an unbuffered pH 5.4 aqueous solution of 0.1 M KCl at an unexpanded mercury drop (solid curve), and after drop expansion by a factor of 1.28 (dashed curve) and of 1.57 (dot-dashed curve).

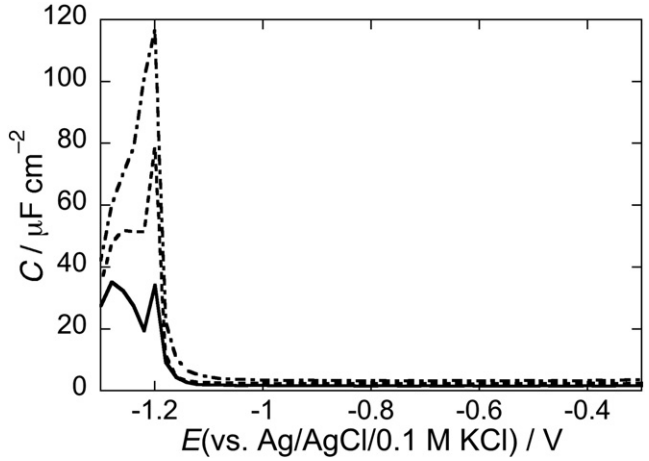

Fig. 2. AC voltammograms at 75 Hz of a Hg-supported DOPS SAM in an unbuffered pH 5.4 aqueous solution of 0.1 M KCl at an unexpanded mercury drop (solid curve), and after drop expansion by a factor of 1.28 (dashed curve) and of 1.57 (dot-dashed curve).

deprotonation. In fact, surface dipole potential measurements carried out by drop expansion in unbuffered solution yield a value of about +0.150 V, practically equal to that obtained by the same measurements for the DOPC monolayer, and ascribable to the ester linkages of the glycerol backbone [36]. If phosphate deprotonation took place during drop expansion, if would cause an appreciable change in the surface dipole potential with respect to that of DOPC. As a sufficiently strong electric field forces the dipolar heads to align normally to the monolayer plane, the exposition of the protonated phosphate group to the aqueous solution is expected to cause its deprotonation. This might possibly cause a back and forth movement of protons along the polar heads following the AC signal, with a resulting increase in the pseudocapacitance peak.

The effect of SR-E upon a mercury-supported DOPC SAM was investigated at pH 3, 5.4 and 7. Incidentally, the capacitance of a pure DOPC SAM is independent of pH. The first two peaks of the AC voltammogram of the DOPC SAM, as recorded immediately after addition of 0.5 μM SR-E, followed by a rapid solution stirring and four consecutive voltage scans, were only slightly affected at pH 3 and practically unaffected at pH 5.4 and 7 (Fig. 3). However, if a series of impedance spectra is first recorded along the whole flat capacitance minimum in the presence of 0.5 μM SR-E, the subsequent AC voltammogram is characterized by the almost complete suppression of the peaks at pH 3 and 5.4, whereas at pH 7 the peaks are only slightly decreased. This behavior indicates that the SR-E molecules in solution do not interact directly with the polar heads when coming in contact with them from the aqueous solution. Only their intercalation with the lipid monolayer, induced by a prolonged permanence over a broad potential range under electrochemical impedance spectroscopy conditions, has an effect; the intercalation prevents cooperative reorientation of the DOPC molecules causing peak suppression. The attack of the positively charged SR-E to the DOPC monolayer is probably similar to that made by polyvalent cations of lanthanides to phosphatidylcholine (PC) vesicles. The ^{1}H, ^{31}P and ^{13}C NMR spectra of PC vesicles in the presence of these cations seem to point to a change in the orientation of the trimethylammonium-phosphate dipoles from parallel to the bilayer plane to tilted by about 45° [37,39]. The pH dependence of the intercalation of the SR-E molecules is consistent with this hypothesis. Thus, the phosphate group of DOPC is partially protonated at pH 3 and becomes completely deprotonated at pH > 4 [37]. The stability of the planar orientation of the trimethylammonium-phosphate dipoles is clearly decreased by the presence of protonated phosphate groups, which cannot interact electrostatically with neighboring trimethylammonium groups. Hence, the SR-E attack to the DOPC monolayer will be more effective at lower pH values, also in view of the fact that

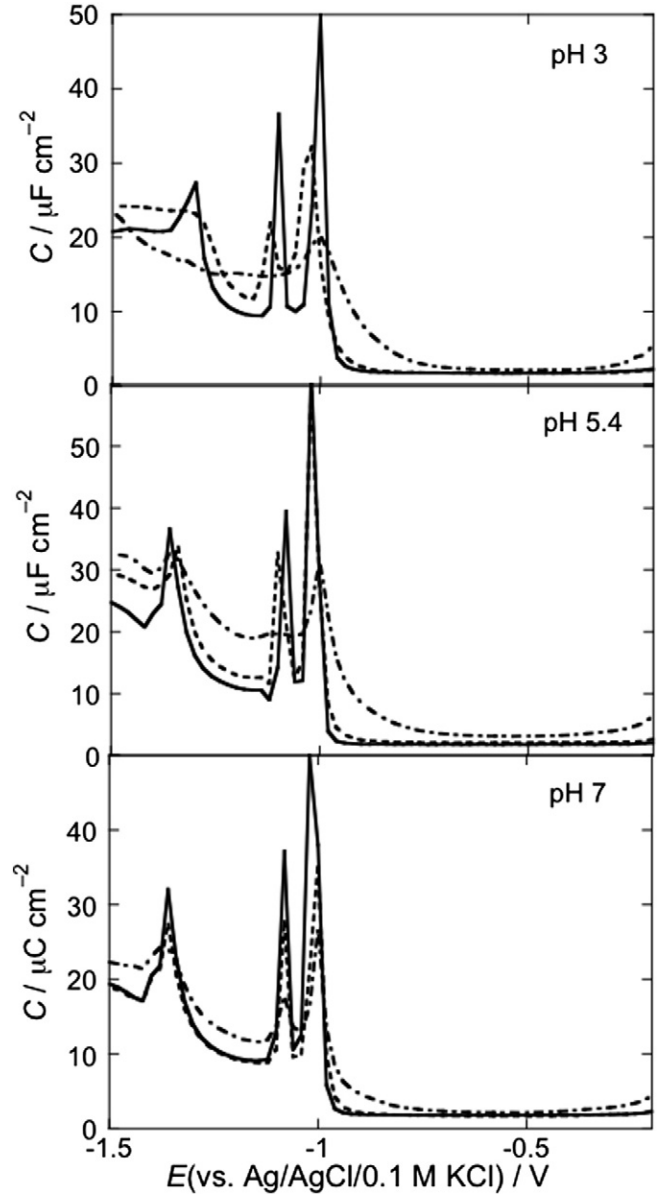

Fig. 3. AC voltammograms at 75 Hz of Hg-supported DOPC SAMs in pH 3, pH 5.4 (unbuffered) and pH 7 solutions of 0.1 M KCl in the absence of SR-E (solid curves), immediately after addition of 0.5 μM SR-E (dashed curves) and after recording a series of impedance spectra (dot-dashed curves).

SR-E has a charge close to +3 at pH 3 and +2 at higher pH values. The attack is likely to occur by H-bond formation between one of the three SR-E amino groups and a DOPC phosphate group. A similar effect is observed upon replacing 0.1 M KCl by 0.05 M $CaCl_2$ (data not shown).

The effect of SR-E on the DOPS monolayer in 0.1 M KCl differs from that on the DOPC monolayer mainly because it is immediately felt upon recording a few AC voltammograms after SR-E addition to the aqueous solution. SR-E depresses the pseudocapacitance peak, whereas it eliminates it completely after recording an impedance spectrum over the stability range of the DOPS monolayer, as shown in Fig. 4. The effect of SR-E is more pronounced at pH 3 than in unbuffered solution of pH 5.4. Replacing 0.1 M KCl by 0.05 M $CaCl_2$ enhances the effect of SR-E on DOPS at pH 5.4, making it comparable with that in 0.1 M KCl at pH 3 (data not shown). The effect of SR-E occurring more rapidly on the DOPS monolayer than on the DOPC one is to be ascribed to the ease with which the DOPS monolayer may change its rather complex conformation. The "camaleontic" adaptability of the DOPS conformation

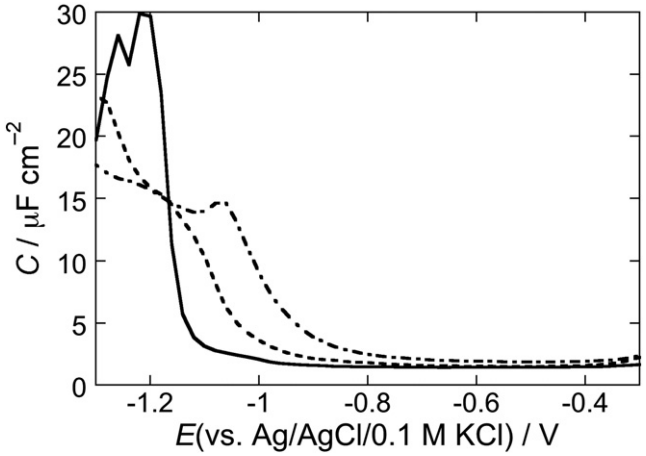

Fig. 4. AC voltammograms at 75 Hz of a Hg-supported DOPS SAM in a pH 5.4 unbuffered solution of 0.1 M KCl in the absence of SR-E (solid curve), immediately after addition of 0.5 μM SR-E (dashed curve) and after recording a series of impedance spectra (dot-dashed curve).

to even slightly different environmental conditions is testified by the notable scatter in the pK values of its carboxyl and phosphate groups reported in the literature [37]. The protonated state of the phosphate groups of DOPS, which is a maximum at low pH values, is endangered by any exogenous species capable of disrupting the planar arrangement of the carboxyl–amino dipoles between adjacent DOPS molecules. This is particularly true for calcium ion, which has a high affinity for the deprotonated phosphate group and may shift the equilibrium from the protonated to the deprotonated form. A similar effect may possibly be exerted by SR-E, which can form H-bonds between its amino groups and the deprotonated phosphate groups in equilibrium with the still protonated ones.

3.2. Effect of SR-E on tBLMs

In Section 3.1, phospholipid SAMs were investigated using AC voltammetry, a phase-sensitive technique particularly convenient for recording pseudocapacitance peaks. In investigating tBLMs, use was made of potential-step chronocoulometry, the technique of choice for monitoring the time dependence of the ionic charge that accumulates in the hydrophilic spacer at constant applied potential. TBLMs were also interrogated using cyclic voltammetry, the most appropriate technique for monitoring the flow of translocating ions in and out of the hydrophilic spacer.

3.2.1. Chronocoulometric behavior

The charge Q flowing at a DPTL/DOPS tBLM in a pH 3 aqueous solution of 0.1 M KCl and 0.8 μM SR-E, as a consequence of a series of potential jumps from a fixed initial potential $E_i = -0.30$ V to more negative final potentials E_f, was recorded as a function of time t. The final potentials were made progressively more negative by −50 mV increments. The presence of 0.8 μM SR-E starts causing an increase in charge over the background value at −0.90 V, as shown by curve *a* in Fig. 5. This is due to an inflow of K^+ ions into the spacer and/or an outflow of Cl^- ions. The charge transient exhibits two inflection points, namely two subsequent sigmoidal charge steps very close to each other. Inflection points in the charge transients correspond to current peaks in the relative current transients, which are reported on the upper part of Fig. 5. In fact, the differentiable function $Q(t)$ has an inflection point of coordinates $(Q(t),t)$ if, and only if, its first derivative, $j = dQ/dt$, has an isolated extremum at t. The occurrence of two inflection points in the Q vs. t curves is clearly highlighted by the presence of two maxima in the corresponding j vs. t curves. The height of the overall two-stage charge step, as measured from the background charge, ranges from

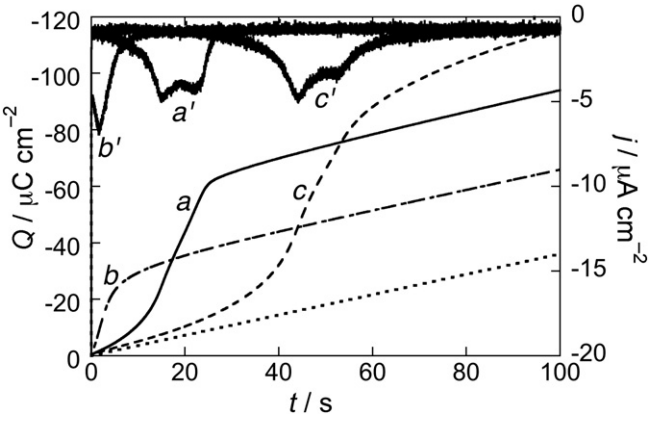

Fig. 5. Charge transients following potential jumps from $E_i = -0.30$ V to -0.90 V at a DPTL/DOPS tBLM in a pH 3 solution of 0.1 M KCl and 0.8 μM SR-E; pristine potential jump (*a*), after a rest time of 30 s at E_i (*b*) and after a further rest time of 300 s at E_i (*c*). The curves *a′*, *b′* and *c′* are the corresponding current transients. The dotted curve is the charge transient from −0.30 V to −0.90 V in the absence of SR-E under otherwise identical conditions.

-45 to -50 μC cm^{-2}. It corresponds to the maximum charge of K^+ ions that can be accommodated in the hydrophilic spacer of the DPTL thiolipid [23]. The plateau of the charge transient is attained at shorter times the more negative the final potential E_f is (data not shown).

If the rest time, τ, at E_i interposed between two consecutive identical potential jumps is 30 s, the long foot that precedes the charge step is completely absent, the plateau is reduced by about half and only a single inflection point is observed (see curve *b* in Fig. 5). This indicates that a rest time τ of 30 s is insufficient to expel all ions from the hydrophilic spacer. After a further rest time τ of 300 s at E_i, a subsequent potential jump to −0.90 V yields a charge transient practically identical with the pristine one, albeit with a longer foot (see curve *c* in Fig. 5).

If a potential jump to E_f values more negative than −0.90 V is immediately followed by a further potential jump from E_i to an E_f value of −0.75 V, a sigmoidal charge step with a single inflection point is obtained, as shown by curve *b* in Fig. 6. Importantly, no charge step would be obtained if the $E_i \rightarrow -0.75$ V potential jump were not immediately preceded by a potential jump negative enough to fill the hydrophilic spacer by K^+ ions. The charge step of curve *b* in Fig. 6 has practically the same height as the first sigmoidal stage of the overall two-stage charge step of curves *a* and *c* in Fig. 5, but it is not followed by the second stage, at least over a time period of 100 s. If a further $E_i \rightarrow -0.75$ V potential jump is carried out after a rest time τ of 100 s at E_i, the same sigmoidal charge step is obtained, albeit with a much longer foot (see curve *c* in Fig. 6). This behavior suggests that the SR-E channel triggered by a pristine potential jump to an E_f value negative of −0.90 V is not disrupted for rest times τ at E_i as long as 100 s and may also allow an ion flow along the channel by immediately jumping from E_i to a less negative final potential E_f.

A similar chronocoulometric behavior was observed for the DPTL/DOPC tBLM in a pH 5.4 unbuffered solution of 0.1 M KCl and 0.8 μM SR-E. Thus, upon carrying out potential jumps from $E_i = -0.30$ V to progressively more negative potentials E_f by −50 mV increments, a charge transient with a long foot and a sigmoidal charge step, about 20 μC cm^{-2} in height, is only attained for $E_f = -0.90$ V (curve *a* in Fig. 7). At t > 60 s, this curve shows an embryo of a second charge step. Repeated potential jumps to $E_f = -0.90$ V, each preceded by a rest time τ of 30 s at E_i, cause the appearance and the progressive increase of a second sigmoidal charge step, until ultimately a two-stage overall charge transient, −45 μC cm^{-2} in height, is attained, which corresponds to complete saturation of the spacer by K^+ ions (see curve *b* in Fig. 7). A potential jump from E_i to −0.75 V carried out immediately after a potential jump to −1.0 V yields a charge transient identical with that observed in the absence of SR-E, as distinct from the behavior observed at a DPTL/DOPS tBLM at pH 3 (Fig. 6). As a whole, the two-stage behavior of the charge transients induced by SR-E at a DPTL/DOPC tBLM at pH 5.4 is slightly less pronounced than the one occurring at a DPTL/DOPS tBLM at pH 3. A still less pronounced, albeit clearly detectable, two-stage chronocoulometric behavior is induced by SR-E at a DPTL/DOPC tBLM at pH 3 (data not shown).

At variance with the previous systems, no two-stage charge transients are observed at a DPTL/DOPS tBLM in a pH 5.4 unbuffered solution of 0.1 M KCl and 0.8 μM SR-E. Potential jumps from E_i to progressively more negative final potentials E_f in the presence of SR-E start yielding charge transients distinctly different from those in its absence only for E_f more negative than −0.80 V (Fig. 8). The resulting charge steps have a sigmoidal shape with only a single inflection point and a height of about −45 μC cm^{-2}, corresponding to spacer saturation by K^+ ion. The presence of a single sigmoidal charge step is apparent from the corresponding current transients, which show only a single peak. As expected, the plateau of the transients is attained at progressively shorter times, the more negative the E_f value is.

3.2.2. Cyclic voltammetric behavior

The steady-state cyclic voltammogram of a DPTL/DOPS tBLM in a pH 3 aqueous solution of 0.1 M KCl and 0.8 μM SR-E, as recorded by

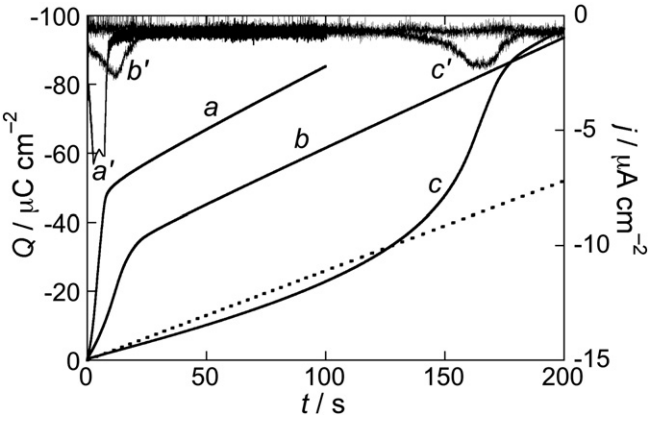

Fig. 6. Charge transients following potential jumps from $E_i = -0.30$ V to different final potentials E_f at a DPTL/DOPS tBLM in a pH 3 solution of 0.1 M KCl and 0.8 μM SR-E; pristine potential jump to $E_f = -1.00$ (*a*), subsequent potential jump to −0.75 V after a rest time of 30 s at E_i (*b*) and after a further rest time of 300 s at E_i (*c*). The curves *a′*, *b′* and *c′* are the corresponding current transients. The dotted curve is the charge transient from −0.30 V to −1.00 V in the absence of SR-E under otherwise identical conditions.

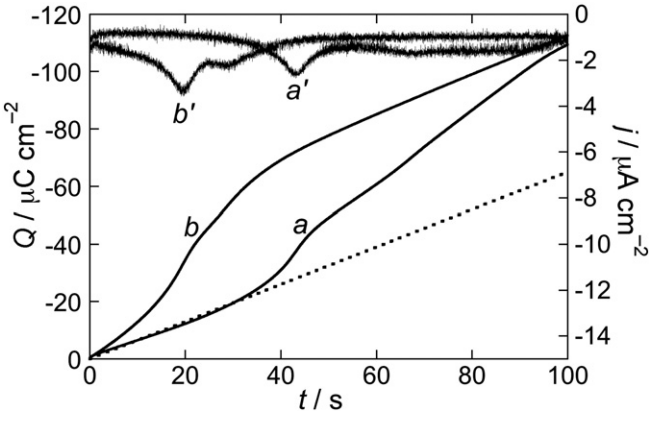

Fig. 7. Charge transients following potential jumps from $E_i = -0.30$ V to $E_f = -0.90$ V at a DPTL/DOPC tBLM in a pH 5.4 unbuffered solution of 0.1 M KCl and 0.8 μM SR-E; pristine potential jump to $E_f = -0.90$ V (*a*), potential jump to $E_f = -0.90$ V obtained after repeated identical potential jumps, each preceded by a rest time of 30 s at E_i. The dotted curve is the charge transient from −0.30 V to −0.90 V in the absence of SR-E under otherwise identical conditions.

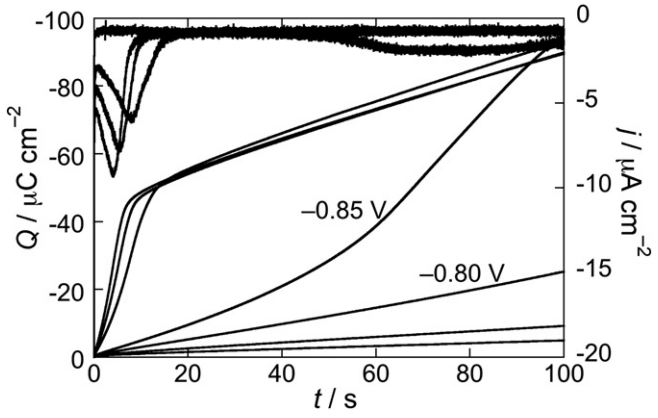

Fig. 8. Charge transients following potential jumps from $E_i = -0.30$ V to progressively more negative final potentials E_f, which vary from −0.70 V to −1.00 V by −50 mV increments, at a DPTL/DOPS tBLM in a pH 5.4 unbuffered solution of 0.1 M KCl and 0.8 μM SR-E. The slope of the charge transients increases progressively with a negative shift in E_f. The four current transients correspond to the charge transients from −0.85 V to −1.00 V.

scanning the potential between −0.20 V and −0.90 V at a scan rate of 10 mV/s, shows a negative peak at about −0.72 V, followed by a shoulder (see the solid curve in the inset of Fig. 9). The corresponding positive current is flat and distributed almost uniformly at potentials positive of −0.65 V. The overall charge under the negative peak and the shoulder amounts to about −20 μC cm^{-2}. An increase in the scan rate to 50 mV/s converts the negative peak into a shoulder and the shoulder into a rounded peak, as shown by the dashed curve in the inset of Fig. 9, and causes the charge obtained by integration of the negative current to decrease to −10 μC cm^{-2}.

A similar steady-state cyclic voltammogram, with a negative peak followed by a shoulder, is also provided by a DPTL/DOPC tBLM in a pH 5.4 unbuffered solution of 0.1 M KCl and 0.8 μM SR-E (Fig. 9). The negative peak is shifted by about 150 mV toward more negative potentials with respect to that at a DPTL/DOPS tBLM at pH 3. The presence of a negative peak and of a subsequent shoulder in the cyclic voltammograms of the DPTL/DOPS tBLM in pH 3 aqueous 0.1 M KCl and of the DPTL/DOPC tBLM in pH 5.4 aqueous 0.1 M KCl, both in the presence of 0.8 μM SR-E, are to be related to the two-stage charge transients provided by these two systems. In keeping with this statement, the DPTL/DOPS tBLM in a pH 5.4 unbuffered solution of 0.1 M KCl and 0.8 μM SR-E, which provides a single sigmoidal charge transient, yields a cyclic voltammogram with a single sharp negative current peak and a flat positive current, as appears from the solid curve in Fig. 10. At a scan rate of 10 mV/s, the charge under the negative current peak amounts to about −40 μC cm^{-2}. Interestingly, addition of 0.5 mM $CaCl_2$ to the solution bathing the tBLM suppresses the current induced by SR-E (see the dotted curve in Fig. 10). Calcium ions exert an analogous suppressive effect on DPTL/DOPS and DPTL/DOPC tBLMs at pH 3. This behavior can be tentatively explained by calcium ions binding to the carboxyl groups of the SR-E molecules that line the mouth of the SR-E channel, similarly to their binding to the carboxyl groups of human erythrocyte membranes [40]. However, at potentials negative of −0.90 V, calcium ions move across the lipid bilayer moiety in the presence of SR-E, yielding a sharp and high negative cyclic voltammetric peak (data not shown). Their presence also contributes to increasing the height of chronocoulometric charge steps for $E_f = -1.0$ V beyond the −45 μC cm^{-2} value observed in 0.1 M KCl (data not shown), in view of their higher charge number with respect to K^+ ions.

Cyclic voltammetry was also used to test the selectivity of DPTL/DOPC and DPTL/DOPS tBLMs toward the chloride ion. To this end, use was made of an aqueous solution of 0.04 M Na_2H_2ATP salt, brought to pH 5.5 by a small addition of NaOH. The ATP anion is known not to permeate biomembranes. Hence, if a peptide channel is highly selective toward chloride ion, as is the case with the small protein sarcolipin [41], its incorporation in a tBLM will not allow ion flow across the lipid bilayer moiety. Conversely, an appreciable anion flow will be observed upon diluting the 0.04 M Na_2H_2ATP solution with a 0.08 M NaCl solution. Fig. 11 shows the cyclic voltammogram of a DPTL/DOPC tBLM in a pH 5.5 solution of 0.04 M Na_2H_2ATP and 0.8 μM SR-E before (dotted curve) and after the further dilution with 0.08 M NaCl (solid curve). It is evident that no ion flow occurs in the presence of sodium ions, whereas a cyclic voltammogram with a sharp negative current peak at −0.97 V and a flat positive current hump is recorded upon addition of chloride ions. At a scan rate of 50 mV/s, the charge under the negative current peak amounts to −15 μC cm^{-2}. This points to a high selectivity of the SR-E channel incorporated in a DPTL/DOPC tBLM for chloride ions. The anion selectivity of the DPTL/DOPC tBLM turns out to be apparently lower when using electrochemical impedance spectroscopy. Thus, the Nyquist plot of this tBLM in 0.04 M Na_2H_2ATP at −0.70 V yields a resistance that is reduced to half upon addition of 1 μg/mL SR-E and to one fourth upon a further dilution with 0.08 M NaCl. This is due to the time required to record a whole impedance spectrum being much longer than that required to record a cyclic voltammogram. Since the chloride transfer number at a DPTL/DOPC tBLM incorporating SR-E is

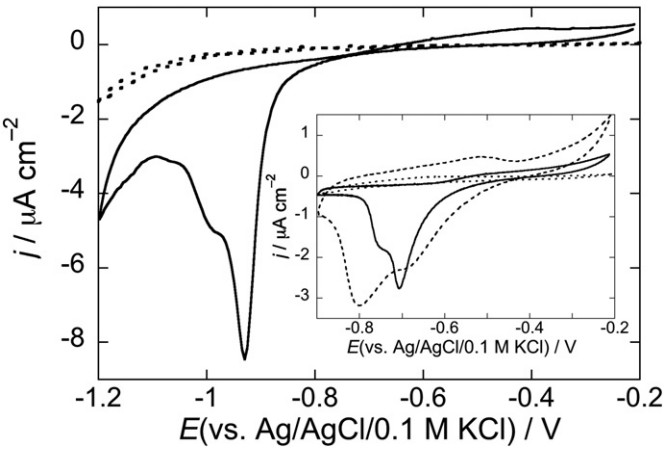

Fig. 9. Cyclic voltammogram of a DPTL/DOPC tBLM in a pH 5.4 unbuffered solution of 0.1 M KCl in the absence (dotted curve) and in the presence of 0.8 μM SR-E (solid curve) at a scan rate of 50 mV/s. The inset is the cyclic voltammogram of a DPTL/DOPS tBLM in a pH 3 solution of 0.1 M KCl in the absence (dotted curve) and in the presence of 0.8 μM SR-E at a scan rate of 10 mV/s (solid curve) and 50 mV/s (dashed curve).

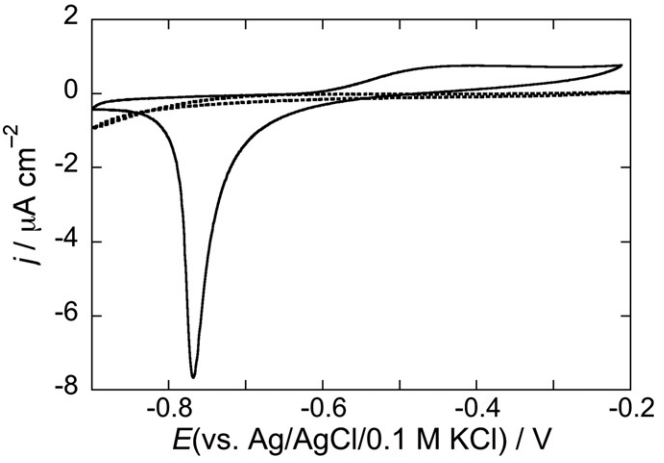

Fig. 10. Cyclic voltammogram of a DPTL/DOPS tBLM in a pH 5.4 unbuffered solution of 0.1 M KCl and 0.8 μM SR-E at a scan rate of 10 mV/s before (solid curve) and after addition of 10^{-3} M Ca^{2+} (dotted curve). The cyclic voltammogram in the absence of SR-E and Ca^{2+} under otherwise identical conditions coincides with the dotted curve, within the limits of experimental error.

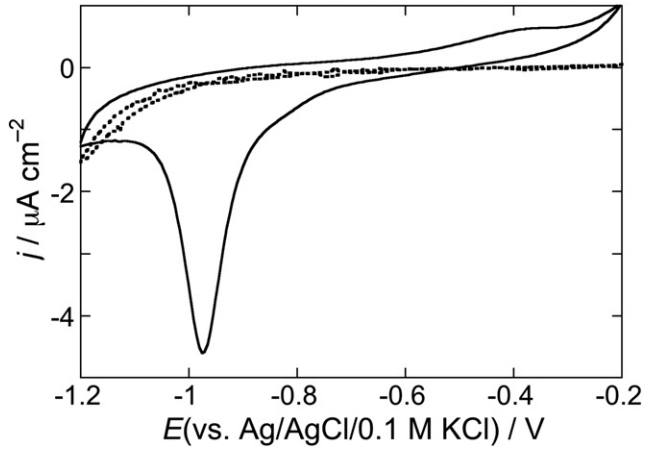

Fig. 11. Cyclic voltammogram of a DPTL/DOPC tBLM in a pH 5.5 solution of 0.04 M Na_2H_2ATP and 0.8 μM SR-E at a scan rate of 50 mV/s (dotted curve) and upon dilution with 0.08 M NaCl (solid curve). The cyclic voltammogram in the absence of SR-E and NaCl under otherwise identical conditions coincides with the dotted curve, within the limits of experimental error.

not exactly unitary, a longer time allows a higher number of sodium ions to move along the SR-E channel into the spacer before NaCl addition.

As distinct from a DPTL/DOPC tBLM, a DPTL/DOPS tBLM in a pH 5.5 solution of 0.04 M Na_2H_2ATP lacking chloride ions yields a cyclic voltammogram analogous to that shown by the solid curve in Fig. 11, with the negative peak shifted by about 100 mV toward less negative potentials with respect to that in the latter curve (data not shown). Addition of 0.08 M NaCl leaves the cyclic voltammogram practically unaltered. This indicates that the anion selectivity of the SR-E channel incorporated in a DPTL/DOPS tBLM, if any, is too low to be detected by the rather crude procedure based on the use of the ATP salt. The above results agree with the high anion transfer number of 0.97 for NaCl at a DOPC BLM [14], to be compared with a value of 0.73 at a DOPS BLM [10].

4. Discussion

For a comparison with the results obtained at conventional BLMs, it is important to provide an extra-thermodynamic estimate of the potential difference across the lipid bilayer moiety of the Hg-supported tBLM, namely the intramembrane potential ϕ_{im}. On the basis of a number of different pieces of experimental evidence, it was concluded that ϕ_{im} for a DPTL/DOPC tBLM in aqueous 0.1 KCl in the absence of ions in the hydrophilic spacer equals zero at an applied potential of about −0.48 V/SCE, and hence at about −0.52 V vs. the Ag/AgCl/(0.1 M KCl) reference electrode [42]. The latter potential coincides with the midpoint potential between the negative and the positive peak of the stabilized cyclic voltammogram of a DPTL/DOPC tBLM incorporating the ohmic channel gramicidin from its 0.3 μM solution in unbuffered aqueous 0.1 M KCl [29]. The shape of this cyclic voltammogram is typical for ohmic channels, being roughly centrosymmetric, with the inversion center located at the midpoint potential (see Fig. 17 in Ref. [43]). The midpoint potential for a cyclic voltammogram at a DPTL/DOPC tBLM provided by an ohmic ion channel selective toward a cation, such as gramicidin, is the potential at which the cation inflow into the spacer matches the cation outflow, giving rise to a zero net current. Hence, it can be regarded as a reliable estimate of the zero intramembrane potential.

Surprisingly, we recently verified that the midpoint potential at a DPTL/DOPS tBLM incorporating gramicidin from its 0.1 μM solution in 0.1 M KCl depends on pH (unpublished results). Thus, a decrease in pH causes a positive shift in the midpoint potential and a gradual decrease in the separation between the positive and negative peak potentials. The midpoint potential, corresponding to a zero intramembrane potential ϕ_{im}, amounts to about −0.66 V at pH 7, −0.55 V in a pH 5.4 unbuffered solution, and −0.44 V at pH 3. Practically identical midpoint potential values were obtained at a DPTL/DOPC tBLM under otherwise identical conditions. Even more surprisingly, the potential at which the current at a DPTL/DOPC tBLM or DPTL/DOPS tBLM incorporating SR-E from its 0.8 μM solution in 0.1 M KCl intersects the corresponding background current varies with pH, assuming values very close to those for the midpoint potential of the gramicidin peaks at the same tBLMs. Since gramicidin is neutral whereas SR-E is positively charged, this effect is expected to depend more on the lipid than on the ion channel. It is possible that the mouth of a channel may drag ionizable and/or dipolar groups of the lipid polar heads well inside the polar head region (even if exposed to the aqueous solution and screened by it at a sufficient distance from the ion channel mouth). This would generate a local nonzero potential difference, if nonexisting in the absence of the channel, or it would modify it, if already existing. It is also possible that the very movement of the ions passing through the mouth of a channel during their translocation may transiently determine such a local alteration of the lipid polar head conformation.

In light of the above results, the positive shift by about 150 mV in the negative peak potential of the cyclic voltammogram in passing from a DPTL/DOPC tBLM incorporating SR-E at pH 5.4 to a DPTL/DOPS tBLM at pH 3 (cf. Fig. 9 and its inset) is mainly to be ascribed to a concomitant shift in the zero intramembrane potential. In view of the position of the corresponding zero ϕ_{im} values, the negative peaks in Fig. 9 and in its inset fall at intramembrane potentials ranging from −300 to −400 mV, and hence somewhat outside the range of physiological transmembrane potentials of BLMs. It should be noted that the intramembrane potential of a tBLM is the potential difference across its hydrocarbon tail region, whereas the transmembrane potential of a BLM is the potential difference between the bulk phases that bath its two sides. In a symmetrical BLM interposed between two identical aqueous solutions, transmembrane potential and intramembrane potential coincide, because the surface dipole potentials on the two sides of the hydrocarbon tail region counterbalance each other, but only if any ion channels are symmetrically incorporated in the BLM, so as not to generate sidedness; this is not the case with SR-E. The non-physiological intramembrane potentials required for ion flow in tBLMs are in apparent contrast with the currents at conventional BLMs incorporating SR-E in field-reversal experiments, which flow at transmembrane potentials ranging from ±120 to ± 200 mV [10,14]. The higher ϕ_{im} values required to activate the SR-E channels at tBLMs have to be ascribed to the fixed proximal monolayer of phytanyl hydrocarbon tails bound via ether linkages to the tetraethyleneoxy spacer. This monolayer has practically no polar heads. Conversely, the movement of the polar heads on the opposite side of a conventional DOPS BLM with respect to SR-E addition (i.e., the *trans* side) was considered by Malev et al. [14] to play a major role in favoring SR-E channel opening in a pH 6 aqueous solution of 0.1 M NaCl, when the transmembrane potential was negative on the *trans* side. The opening of the SR-E ion channel was tentatively ascribed to an electrostatic pushing of the negatively charged DOPS polar heads of the *trans* lipid leaflet toward the interior of the lipid bilayer, so as to line the *trans* side of the SR-E channel. This should not be counterbalanced by an analogous pushing of the DOPS polar heads of the *cis* leaflet away from the bilayer because of their lower number, due to the presence of the positively charged lactone rings forming the SR-E channel mouth [14].

In spite of the different structures of BLMs and tBLMs, some similarities in the behavior of SR-E channels in these two different biomimetic membranes are clearly apparent. A peculiar feature of SR-E incorporated in Hg-supported tBLMs consists in the two-stage sigmoidal chronocoulometric charge transients recorded with DPTL/DOPC tBLMs at pH 3 and 5.4, and with DPTL/DOPS tBLMs at pH 3. Conversely, DPTL/DOPS tBLMs at pH 5.4 yield charge transients characterized by a single sigmoidal charge step. The two-stage sigmoidal behavior contrasts with all potential-jump chronocoulometric measurements

carried out at these tBLMs upon incorporating several channel-forming peptides [27–29,31,41] from aqueous 0.1 M KCl. In all these cases, a single sigmoidal charge step, about 45 μC cm^{-2} high, was recorded, by jumping from an initial potential E_i ranging from −0.20 to −0.30 V to sufficiently negative final potentials E_f. These E_i values correspond to positive intramembrane potentials, ϕ_{im}, as measured from the mercury side of the bilayer. They should be compared with the transmembrane potentials on the side of conventional BLMs opposite to that where SR-E is added, taken as the *cis* side. It is worth noting that the peculiar two-stage sigmoidal charge transients are observed in 0.1 M KCl at tBLMs with a distal DOPC monolayer at pH 5.4 and with a distal DOPS monolayer at pH 3, under experimental conditions close to those at which the SR-E incorporated in the corresponding diphytanoylphosphatidylcholine (DPhPC) [14] and DOPS [10,14] BLMs have been reported to be open at negative transmembrane potentials on the *trans* side. On the other hand, single sigmoidal charge transients are observed at tBLMs with a distal DOPS monolayer in pH 5.4 aqueous 0.1 M KCl, under experimental conditions close to those at which the corresponding DOPS BLMs have been reported to be open at positive transmembrane values on the *trans* side [10,14]. Even though Hg-supported tBLMs are highly asymmetrical, while the BLMs employed in SR-E measurements are symmetrical, the above similarities could hardly be regarded as fortuitous.

In consideration of the results on BLMs by Malev and coworkers [14], we will assume that the SR-E channels incorporated in DPTL/DOPC tBLMs in 0.1 M KCl at pH 3 and 5.4, and in DPTL/DOPS tBLMs at pH 3, are in a "potentially" open state at $E_i = -0.30$ V. In spite of this assumption, our measurements exclude that they may allow an ion flow across the lipid bilayer moiety while resting at E_i. If this were the case, then the SR-E channels would allow a flow of chloride ions into the hydrophilic spacer at E_i. A subsequent potential jump to a sufficiently negative E_f value would then yield an overall two-stage charge transient involving a charge appreciably greater than −45 μC cm^{-2}, which corresponds to spacer saturation by potassium ions. In fact, such a charge transient would also include a charge density of the same sign due to an outflow of chloride ions concomitant with the inflow of potassium ions. Moreover, the sigmoidal shape of the charge transients is indicative of the formation of SR-E channels by a mechanism of nucleation and growth during the negative potential jump from E_i to E_f [27]. We may tentatively hypothesize that the SR-E molecules retain a memory of their potentially open state at E_i during channel formation following the potential jump, thereby opening during the first stage of the charge transient at E_f and then starting to close before the spacer is saturated by potassium ions. A form of memory is not only present in sodium ion channels, but also in the ion channel formed by the microcyclic polyol lactone monazomycin in BLMs [44]. Conversely, the SR-E channels incorporated in a DPTL/DOPS tBLM at pH 5.6, which are expected to be close at E_i in view of the results at BLMs [10,14], will start to open at negative final potentials E_f, like the other biomimetic systems, but they will have no tendency to close. This will allow the spacer to be fully saturated by potassium ions in a one-stage sigmoidal charge transient. In all cases, the backward potential jump from E_f to E_i involves only the charge due to the expulsion of K^+ ions from the spacer, indicating that Cl^- ions are not allowed to enter the spacer during this jump. This is quite probably due to the outflow of K^+ ions hindering a concomitant inflow of Cl^- ions. This behavior points to the propensity of SR-E to favor K^+ ion flow, in agreement with the increase in K^+ efflux from plant and yeast cells induced by this lipodepsipeptide [6–47].

The tendency of the SR-E channels incorporated in DPTL/DOPC tBLMs at pH 3 and 5.4 and in DPTL/DOPS at pH 3 to reopen after starting to close can possibly be justified on the basis of some rough modelistic considerations. The analysis of the electrochemical impedance spectra of a DPTL/DOPC tBLM incorporating the gramicidin ohmic channel from aqueous 0.1 M KCl reveals that the capacitance, C_{il}, of the "inner layer" interposed between the charge density on the mercury surface and that, Q, on the ions stored in the hydrophilic spacer increases almost linearly with the latter charge, attaining a value of about 200 μF cm^{-2} when Q attains its maximum saturation value of +45 μC cm^{-2} [17]. In practice, the charge density on the metal is almost equal in magnitude and opposite in sign to Q. In fact, the charge density due to diffuse layer ions is almost negligible with respect to $|Q|$, and the potential difference across the diffuse layer is accordingly negligible, also in view of the high value of the diffuse-layer capacitance [23]. Incidentally, it is thanks to the high inner layer capacitance C_{il} that the filling of the hydrophilic spacer by K^+ ions requires a few hundreds of mV to occur, rather than several volts, as would be required if the capacitance were identified with that, ~3 μF cm^{-2}, of the lipoic acid residue in the absence of ions in the spacer [48]. The extra-thermodynamic absolute potential difference, $\Delta\phi$, across the whole mercury/solution interface can then be approximately expressed by the equation:

$$\Delta\phi \cong -Q/C_{il} + \chi_S + \phi_{im} + \sigma_i\left(\gamma/\varepsilon_\gamma\varepsilon_0\right) \quad \rightarrow \quad \phi_{im} \cong \Delta\phi + Q/C_{il} - \chi_S - \sigma_i\left(\gamma/\varepsilon_\gamma\varepsilon_0\right) \tag{1}$$

where χ_S is the surface dipole potential of the tetraethyleneoxy spacer and ϕ_{im} is the intramembrane potential. The further term, $\sigma_i(\gamma/\varepsilon_\gamma\varepsilon_0)$, expresses the potential difference across the polar head region of the distal lipid monolayer in the presence of a charge density σ_i due to ionizable groups buried inside the polar heads; γ and ε_γ are the length and the dielectric constant of the polar head region, and ε_0 is the permittivity of free space. A number of pieces of experimental evidence combined with some mild modelistic considerations indicate that χ_S is about equal to −0.230 V and that $\Delta\phi$ is obtained by adding +0.230 V to the applied potential measured vs. the SCE [42], and, hence, by adding +0.190 V to the Ag/AgCl/0.1 M KCl reference electrode. Setting Q = +45 μC cm^{-2}, C_{il} = 200 μF cm^{-2} and $\sigma_i = 0$, Eq. (1) yields a value of −0.65 V for the potential $E_0 = \Delta\phi - 0.190$ V at which the intramembrane potential ϕ_{im} equals zero. This value is very close to the midpoint potential, −0.66 V, between the negative and the positive peak of the cyclic voltammogram of a DPTL/DOPS tBLM incorporating gramicidin at pH 7 (unpublished results), which is the applied potential at which the intramembrane potential is estimated to be equal to zero. As already pointed out, the above midpoint potential varies with pH. This pH dependence can be ascribed to the $\sigma_i(\gamma/\varepsilon_\gamma\varepsilon_0)$ term in Eq. (1), which can be varied locally at the mouth of ion channels, depending on the nature of the lipid molecules and of the pH value. Worth noting for the present purpose is that a gradual increase in the positive charge Q of potassium ions accommodated in the spacer causes ϕ_{im} to shift toward less negative values at the constant final potential E_f of a potential jump (and, hence, at constant $\Delta\phi$), in view of Eq. (1). This may explain why the SR-E channel incorporated in DPTL/DOPC tBLMs and in the DPTL/DOPS tBLM at pH 3, after opening and then tending to close at E_f, may tend to open again at the same final potential, due to a positive shift of ϕ_{im} resulting from accumulation of potassium ions into the spacer. The time during which the SR-E channel remains in the closed state at the final potential is shorter the more negative the E_f value is. This is probably due to the fact that, as E_f becomes progressively more negative, the increasing electrostatic attraction exerted by the local electric field toward K^+ ions tends to overcome the resistance opposed by a closed ion channel.

The blocking of the SR-E channel by Ca^{2+} ions over the range of physiological intramembrane potentials, as shown in Fig. 10, deserves some additional considerations. SR-E has been reported to induce Ca^{2+} influx in plant [9,49,50] and yeast cells [47]. Takemoto and colleagues provided evidence that SR-E activity is responsible primarily for opening of Ca^{2+} channels in plasma membranes [47,51]. Conversely, Hutchinson et al. [9,50] claimed that transmembrane Ca^{2+} flux is due to SR-E itself forming ion channels. Thus, they state that their "findings in both the erythrocyte lysis assay and using direct measurements in bilayers show that SR-E forms pores that are highly permeable to

Zn^{2+} and Ca^{2+} cations". However, to the best of our knowledge, no direct evidence for Ca^{2+} permeation in artificial bilayers induced by SR-E was provided by these authors. Conversely, our measurements indicate that Ca^{2+} ions inhibit the SR-E channel, in analogy with their effect on the pores of the lipodepsipeptide tolaasin [52]. Accordingly, a re-examination of the biological effects exerted by SR-E has to be accomplished in light of the results presented in this study.

5. Conclusions

This study describes the interaction of SR-E with a highly asymmetrical lipid bilayer, in which the polar heads of the proximal lipid monolayer are practically lacking. The ion flow through the SR-E ion channel incorporated in the lipid bilayer moiety of tBLMs was exclusively dominated by the distal monolayer. This provides useful information on the effect of phospholipid asymmetry of cell membranes on ion channel behavior. The incorporation of SR-E in mercury-supported tBLMs requires nonphysiological intramembrane potentials, as distinct from symmetrical BLMs. However, once incorporated, the SR-E channel remains stable over the range of physiological intramembrane potentials. Under the same experimental conditions at which symmetrical BLMs of DOPC and DOPS incorporating SR-E are open at positive transmembrane potentials, the corresponding distal monolayers of tBLMs allow ion inflow only at non-physiological negative intramembrane potentials and then tend to block it, following a negative potential jump. On the other hand, distal DOPS monolayers of tBLMs incorporating SR-E at pH 5.4 open at negative transmembrane potentials and remain open, following a negative potential jump (Fig. 8), similarly to DOPS BLMs. In all cases, the ion flow at tBLMs induced by negative potential jumps involves exclusively K^+ ions. On the contrary, voltage cycling also induces the flow of Cl^- ions, as appears from the cyclic voltammogram in Fig. 11. Most importantly, the intramembrane potential of the asymmetrical tBLMs with distal DOPC and DOPS monolayers varies appreciably with the solution pH and depends much more on the nature of the lipid than that of the ion channel. This effect, which is exclusively determined by the distal monolayer, is expected to be wiped out in symmetrical BLMs. It sheds some light on the distinct contributions to the transmembrane potential from the two lipid leaflets of cell membranes.

A detailed investigation of the channel-forming activity of syringopeptin 25, another interesting peptide produced by *P. syringae* pv. *syringae*, which forms ion channels exhibiting quasi-ohmic behavior at physiological intramembrane potentials in our mercury-supported tBLMs, is under way. A semi-quantitative interpretation of the positive shift of the intramembrane potential with decreasing pH, as induced by changes in the surface dipole potential of the phospholipid polar heads adjacent to the mouth of the gramicidin ion channel, is also in progress.

Acknowledgements

This study was partially supported by grants from the Italian Ministry of Economy and Finance for the project "Innovazione e sviluppo del Mezzogiorno – Conoscenze Integrate per Sostenibilità ed Innovazione del *Made in Italy* Agroalimentare – Legge n. 191/2009". Thanks are due to Prof. Adrian Schwan (University of Guelph, Guelph, Ontario, Canada) for providing us with the DPTL thiolipid.

References

[1] S.L. Sinden, J.E. De Vay, P.A. Backman, Properties of syringomycin, a wide spectrum antibiotic and phytotoxin produced by *Pseudomonas syringae*, and its role in the bacterial canker disease of peach trees, Physiol. Plant Pathol. 1 (1971) 199–213.
[2] A.J. De Lucca, T.J. Jacks, J. Takemoto, B. Vinyard, J. Peter, E. Navarro, T.J. Walsh, Fungal lethality, binding, and cytotoxicity of syringomycin-E, Antimicrob. Agents Chemother. 43 (1999) 371–373.
[3] A. Segre, R.C. Bachmann, A. Ballio, F. Bossa, I. Grgurina, N.S. Iacobellis, G. Marino, P. Pucci, M. Simmaco, J.Y. Takemoto, The structure of syringomycins A1, E and G, FEBS Lett. 255 (1989) 27–31.
[4] N. Fukuchi, A. Isogai, J. Nakayama, S. Takayama, S. Yamashita, K. Suyama, J.Y. Takemoto, A. Suzuki, Structure and stereochemistry of three phytotoxins, syringomycin, syringotoxin and syringostatin, produced by *Pseudomonas syringae* pv. *syringae*, J. Chem. Soc. Perkin Trans. 1 (1992) 1149–1157.
[5] M. Anselmi, T. Eliseo, L. Zanetti-Polzi, M.R. Fullone, V. Fogliano, A. Di Nola, M. Paci, I. Grgurina, Structure of the lipodepsipeptide syringomycin E in phospholipids and sodium dodecylsulphonate micelle studied by circular dichroism, NMR spectroscopy and molecular dynamics, Biochim. Biophys. Acta 1808 (2011) 2102–2110.
[6] H.H. Reidl, J.Y. Takemoto, Mechanism of action of bacterial phytotoxin syringomycin: simultaneous measurement of early responses in yeast and maize, Biochim. Biophys. Acta 898 (1987) 59–69.
[7] H.H. Reidl, T.A. Grover, J.Y. Takemoto, 31P-NMR evidence for cytoplasmic acidification and phosphate extrusion in syringomycin treated cells of *Rhodotorula pilimanae*, Biochim. Biophys. Acta 1010 (1989) 325–329.
[8] W. Ziegler, J. Pavlovkin, J. Pokorny, Effect of syringotoxin on the permeability of bilayer lipid membranes, Biologia (Bratislava) 39 (1984) 693–699.
[9] M.L. Hutchison, M.A. Tester, D.C. Gross, Role of biosurfactant and ion channel-forming activities of syringomycin in transmembrane ion flux: a model for the mechanism of action in the plantpathogen interaction, Mol. Plant Microbe Interact. 8 (1995) 610–620.
[10] A.M. Feigin, J.Y. Takemoto, R. Wangspa, J.H. Teeter, J.G. Brand, Properties of voltage-gated ion channels formed by syringomycin E in planar lipid bilayers, J. Membr. Biol. 149 (1996) 41–47.
[11] M. Dalla Serra, G. Fagiuoli, P. Nordera, I. Bernhart, C. Della Volpe, D. Di Giorgio, A. Ballio, G. Menestrina, The interaction of lipodepsipeptide toxins from *Pseudomonas syringae* pv. *syringae* with biological and model membranes: a comparison of syringotoxin, syringomycin, and two syringopeptins, Mol. Plant Microbe Interact. 12 (1999) 391–400.
[12] L.V. Schagina, Yu.A. Kaulin, A.M. Feigin, J.Y. Takemoto, J.G. Brand, V.V. Malev, Properties of ionic channels formed by the antibiotic syringomycin E in lipid bilayers: dependence on the electrolyte concentration in the bathing solution, Membr. Cell Biol. 12 (1998) 537–555.
[13] Yu.A. Kaulin, L.V. Schagina, S.M. Bezrukov, V.V. Malev, A.M. Feigin, J.Y. Takemoto, J.H. Teeter, J.G. Brand, Cluster organization of ion channels formed by the antibiotic syringomycin E in bilayer lipid membranes, Biophys. J. 74 (1998) 2918–2925.
[14] V.V. Malev, L.V. Schagina, P.A. Gurnev, J.Y. Takemoto, E.M. Nestorovich, S.M. Bezrukov, Syringomycin E channel: a lipidic pore stabilized by lipopetide? Biophys. J. 82 (2002) 1985–1994.
[15] O.S. Ostroumova, P.A. Gurnev, L.V. Schagina, S.M. Bezrukov, Asymmetry of syringomycin E channel studied by polymer partitioning, FEBS Lett. 581 (2007) 804–808.
[16] V.V. Malev, O.S. Ostroumova, J.Y. Takemoto, L.V. Schagina, Voltage-dependent ion channels induced by cyclic lipodepsipeptides in planar lipid bilayers: structure, properties, and resemblance to native channels, in: A.L. Liu, A. Iglic (Eds.), Advances in Planar Lipid Bilayers and Liposomes, vol. 8, Elsevier, New York, 2008, pp. 59–106 Chap. 3,.
[17] J. Kunze, J. Leitch, A.L. Schwan, R.J. Faragher, R. Naumann, S. Schiller, W. Knoll, J.R. Dutcher, J. Lipkowski, New method to measure packing densities of self-assembled thiolipid monolayers, Langmuir 22 (2006) 5509–5519.
[18] L. Becucci, M.V. Carbone, T. Biagiotti, M. D'Amico, M. Olivotto, R. Guidelli, Incorporation of the HERG potassium channel in a mercury supported lipid bilayer, J. Phys. Chem. B 112 (2008) 1315–1319.
[19] R. Naumann, T. Baumgart, P. Gräber, A. Jonczyk, A. Offenhäusser, W. Knoll, Proton transport through a peptide-tethered bilayer lipid membrane by the H^+-ATP synthase from chloroplasts measured by impedance spectroscopy, Biosens. Bioelectron. 17 (2002) 25–34.
[20] T. Baumgart, M. Kreiter, H. Lauer, R. Naumann, G. Jung, A. Jonczyk, A. Offenhäusser, W. Knoll, Fusion of small unilamellar vesicles onto laterally mixed self-assembled monolayers of thiolipopeptides, J. Colloid Interface Sci. 258 (2003) 298–309.
[21] I.K. Vockenroth, C. Ohm, J.W.F. Robertson, D.J. McGillivray, M. Lösche, I. Köper, Stable insulating tethered bilayer lipid membranes, Biointerphases 3 (2008) FA68–FA72.
[22] J. Leitch, J. Kunze, J.D. Goddard, A.L. Schwan, R.J. Faragher, R. Naumann, W. Knoll, J.R. Dutcher, J. Lipkowski, In situ PM-IRRAS studies of an archaea analogue thiolipid assembled on a Au(111) electrode surface, Langmuir 25 (2009) 10354–10363.
[23] L. Becucci, R. Guidelli, Equilibrium distribution of K^+ ions in the hydrophilic spacer of tethered bilayer lipid membranes, Soft Matter 5 (2009) 2294–2301.
[24] L. Becucci, R. Romero Léon, M.R. Moncelli, P. Rovero, R. Guidelli, Electrochemical investigation of melittin reconstituted into a mercury-supported lipid bilayer, Langmuir 22 (2006) 6644–6650.
[25] L. Becucci, M.R. Moncelli, R. Guidelli, Impedance spectroscopy of OmpF porin reconstituted into a Hg-supported lipid bilayer, Langmuir 22 (2006) 1341–1346.
[26] L. Becucci, A. Santucci, R. Guidelli, Gramicidin conducting dimers in lipid bilayers are stabilized by single-file ionic flux along them, J. Phys. Chem. B 111 (2007) 9814–9820.
[27] L. Becucci, R. Guidelli, Kinetics of channel formation in bilayer lipid membranes (BLMs) and tethered BLMs: monazomycin and melittin, Langmuir 23 (2007) 5601–5608.
[28] L. Becucci, M. Papini, D. Muller, A. Scaloni, G. Veglia, R. Guidelli, Probing membrane permeabilization by the antimicrobial peptide distinctin in mercury-supported biomimetic membranes, Biochim. Biophys. Acta 1808 (2011) 2745–2752.
[29] L. Becucci, F. Maran, R. Guidelli, Probing membrane permeabilization by the antibiotic lipopeptaibol trichogin GA IV in a tethered bilayer lipid membrane, Biochim. Biophys. Acta 1818 (2012) 1656–1662.

[30] L. Becucci, M. Innocenti, S. Bellandi, R. Guidelli, Permeabilization of mercury-supported biomimetic membranes by amphotericin B and the role of calcium ions, Electrochim. Acta 112 (2013) 719–726.
[31] L. Becucci, D. Valensin, M. Innocenti, R. Guidelli, Dermcidin, an anionic antibiotic peptide: influence of lipid charge, pH and Zn^{2+} on its interaction with a biomimetic membrane, Soft Matter 10 (2014) 616–626.
[32] M.R. Moncelli, L. Becucci, A novel model of the hanging mercury drop electrode, J. Electroanal. Chem. 433 (1997) 91–96.
[33] D. Bizzotto, A. Nelson, Continuing electrochemical studies of phospholipid monolayers of dioleoyl phosphatidylcholine at the mercury-electrolyte interface, Langmuir 14 (1998) 6269–6273.
[34] D. Bizzotto, Y. Yang, J.L. Shepherd, R. Stoodley, J. Agak, V. Stauffer, M. Lathuillière, A.S. Akhtar, E. Chung, Electrochemical and spectroelectrochemical characterization of lipid organization in an electric field, J. Electroanal. Chem. 574 (2004) 167–184.
[35] A. Nelson, A. Benton, Phospholipid monolayers at the mercury/water interface, J. Electroanal. Chem. 202 (1986) 253–270.
[36] L. Becucci, M.R. Moncelli, R. Herrero, R. Guidelli, Dipole potentials of monolayers of phosphatidylcholine, phosphatidylserine and phosphatidic acid on mercury, Langmuir 16 (2000) 7694–7700.
[37] M.R. Moncelli, L. Becucci, R. Guidelli, The intrinsic pK_a values for phosphatidylcholine, phosphatidylethanolamine, and phosphatidylserine in monolayers deposited on mercury electrodes, Biophys. J. 66 (1994) 1969–1980.
[38] A. Nelson, F.A.M. Leermakers, Substrate-induced structural changes in electrode-adsorbed lipid layers. Experimental evidence for the behaviour of phospholipid layers on the mercury–water interface, J. Electroanal. Chem. 278 (1990) 73–83.
[39] H. Hauser, M.C. Phillips, B.A. Levine, R.J.P. Williams, Conformation of the lecithin polar group in charged vesicles, Nature 261 (1976) 390–394.
[40] J. Forstner, J.F. Manery, Calcium binding by human erythrocyte membranes. Significance of carboxyl, amino and thiol groups, Biochem. J. 125 (1971) 343–352.
[41] L. Becucci, R. Guidelli, C.B. Karim, D.D. Thomas, G. Veglia, An electrochemical investigation of sarcolipin reconstituted into a mercury-supported lipid bilayer, Biophys. J. 93 (2007) 2678–2687.
[42] R. Guidelli, L. Becucci, Estimate of the potential difference across metal/water interfaces and across the lipid bilayer moiety of biomimetic membranes: an approach, Soft Matter 7 (2011) 2195–2201.
[43] L. Becucci, R. Guidelli, An Electrochemical Platform for Studying Biomembrane Processes. Mercury-Supported Biomimetic Membranes, Lambert Academic Publishing, Saarbrücken, Germany, 2014.
[44] R.U. Muller, C.S. Peskin, The kinetics of monazomycin-induced voltage-dependent conductance. II. Theory and a demonstration of a form of memory, J. Gen. Physiol. 78 (1981) 201–229.
[45] K.A. Mott, J.Y. Takemoto, Syringomycin, a bacterial phytotoxin, closes stomata, Plant Physiol. 90 (1989) 1435–1439.
[46] H. Kauss, T. Waldmann, W. Jeblick, J.Y. Takemoto, The phytotoxin syringomycin elicits Ca^{2+}-dependent callose synthesis in suspension-cultured cells of *Catharanthus roseus*, Physiol. Plant. 81 (1991) 134–138.
[47] J.Y. Takemoto, L. Zhang, N. Taguchi, T. Tachikawa, T. Miyakawa, Mechanism of action of the phytotoxin syringomycin: a resistant mutant of *Saccharomyces cerevisiae* reveals an involvement of Ca^{2+} transport, J. Gen. Microbiol. 137 (1991) 653–659.
[48] L. Becucci, M.R. Moncelli, R. Naumann, R. Guidelli, Potassium ion transport by valinomycin across a Hg-supported lipid bilayer, J. Am. Chem. Soc. 127 (2005) 13316–13323.
[49] J.Y. Takemoto, J.L. Giannini, T. Vassey, D.P. Briskin, Siringomycin effects on plasma membrane Ca2+ transport, in: A. Graniti, R.D. Durbin, A. Ballio (Eds.), Phytotoxins and Plant Pathogenesis, Springer Verlag, Berlin, 1989, pp. 167–175.
[50] M.L. Hutchison, D.C. Gross, Lipopeptide phytotoxins produced by *Pseudomonas syringae* pv. *siringae*: comparison of the biosurfactant and ion-channel forming activities of syringopeptin and syringomycin, Am. Phytopathol. Soc. 10 (1997) 347–354.
[51] J.Y. Takemoto, Bacterial phytotoxin syringomycin and its interaction with host membranes, in: D.P.S. Verma (Ed.), Molecular signals in plant-microbe communications, CRC Press, Boca Raton, Fla, 1992.
[52] P.B. Rainey, C.L. Brodey, K. Johnstone, Biological properties and spectrum of activity of tolaasin, a lipodepsipeptide toxin produced by the mushroom pathogen *Pseudomonas tolaasii*, Physiol. Mol. Plant Pathol. 39 (1991) 57–70.